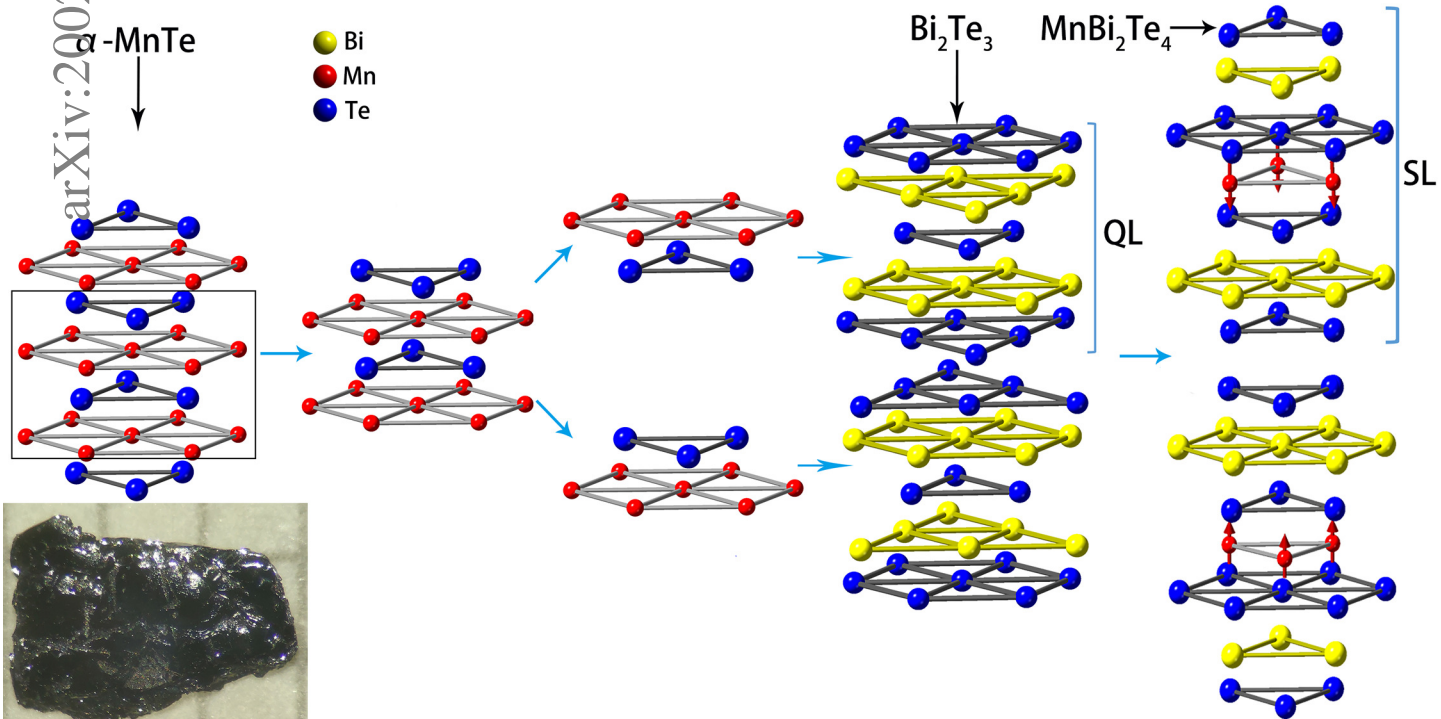


Graphical Abstract

The Layer-inserting Growth of Antiferromagnetic Topological Insulator MnBi_2Te_4 Based on Symmetry and Its X-ray Photoelectron Spectroscopy

Fei Jiao, Jingfeng Wang, Xianyu Wang, Qingyin Tian, Meixia Chang, Lingbo Cai, Shu Zhu, Di Zhang, Qing Lu, Cao Wang, Shugang Tan, Yunlong Li, Jiayuan Hu, Qiang Jing, Bo Liu, Dong Qian



Highlights

The Layer-inserting Growth of Antiferromagnetic Topological Insulator MnBi_2Te_4 Based on Symmetry and Its X-ray Photoelectron Spectroscopy

Fei Jiao, Jingfeng Wang, Xianyu Wang, Qingyin Tian, Meixia Chang, Lingbo Cai, Shu Zhu, Di Zhang, Qing Lu, Cao Wang, Shugang Tan, Yunlong Li, Jiayuan Hu, Qiang Jing, Bo Liu, Dong Qian

- A possible layer-inserting growth mode for antiferromagnetic topological insulator MnBi_2Te_4 is proposed.
- The chemical state of MnBi_2Te_4 has been investigated by XPS.
- The chemical states of Mn and Te in MnBi_2Te_4 agree well with those of $\alpha\text{-MnTe}$.

The Layer-inserting Growth of Antiferromagnetic Topological Insulator MnBi_2Te_4 Based on Symmetry and Its X-ray Photoelectron Spectroscopy

Fei Jiao^{a,d}, Jingfeng Wang^d, Xianyu Wang^{a,d}, Qingyin Tian^d, Meixia Chang^c, Lingbo Cai^d, Shu Zhu^d, Di Zhang^d, Qing Lu^d, Cao Wang^d, Shugang Tan^d, Yunlong Li^b, Jiayuan Hu^b, Qiang Jing^{b,d,*}, Bo Liu^{a,**} and Dong Qian^b

^aSchool of Materials Science and Engineering, Shandong University of Technology, 266 Xincun Xi Road, Zibo, 255000, China

^bKey Laboratory of Artificial Structures and Quantum Control (Ministry of Education), School of Physics and Astronomy, Shanghai Jiao Tong University, Shanghai 200240, China

^cKey Laboratory for Magnetism and Magnetic Materials of Ministry of Education, Lanzhou University

^dLaboratory of Functional Molecules and Materials, School of Physics and Optoelectronic Engineering, Shandong University of Technology, 266 Xincun Xi Road, Zibo, 255000, China

ARTICLE INFO

Keywords:

MnBi_2Te_4

Antiferromagnetic Topological Insulator

XPS

ABSTRACT

The antiferromagnetic topological insulator has attracted lots of attention recently, as its intrinsic magnetism and topological property makes it a potential material to realize the quantum anomalous Hall effect (QAHE) at relative high temperature. Until now, only MnBi_2Te_4 is predicted and grown successfully. The other MB_2T_4 -family materials predicted (MB_2T_4 : M=transition-metal or rare-earth element, B=Bi or Sb, T=Te, Se, or S) with not only antiferromagnetic topological property but also rich and exotic topological quantum states and dynamically stable (or metastable) structure have not been realized on experiment completely. Here, MnBi_2Te_4 single crystals have been grown successfully and tested. It shows typical antiferromagnetic character, with Neel temperature of 24.5K and a spin-flop transition at $H \approx 35000$ Oe, 1.8K. After obtaining MnBi_2Te_4 single crystals, we have tried to synthesize the other members of MB_2T_4 -family materials, but things are not going so well. Then it inspires us to discuss the growth mechanism of MnBi_2Te_4 . The growth mode may be the layer-inserting growth mode based on symmetry, which is supported by our X-ray photoelectron spectroscopy (XPS) measurement. The XPS measurement combing with the A_{r^+} ion sputtering is done to investigate the chemical state of MnBi_2Te_4 . Binding energies (BE) of the MnBi_2Te_4 -related contributions to Mn2p and Te3d spectra agree well with those of inserting material α -MnTe. Rising intensity of the Mn2p satellite for divalent Mn (bound to chalcogen) with atomic number of ligand (from MnO to MnBi_2Te_4) has been observed, thus suggesting classification of MnBi_2Te_4 as the charge-transfer compound. Understanding the growth mode of MnBi_2Te_4 can help us to grow the other members of MB_2T_4 -family materials.

1. Introduction

The milestone discoveries of integer quantum Hall effect (QHE) and fractional QHE made the QHE one of the most important fields in modern condensed matter physics. The dissipationless chiral edge states of the QHE regime can be used in low power consumption, high speed electronic devices. The unique chiral edge states responsible for the QHE originate from the magnetically induced Landau levels[1]. However, well-defined Landau levels are only possible in high-mobility samples under strong external magnetic fields. The demanding requirements prevent the QHE from being widely applied in industry. Therefore, it is highly desirable to achieve the QHE without the need of a strong magnetic field and an extraordinarily high mobility sample. The anomalous Hall effect (AHE) in a ferromagnet can be induced by spontaneous magnetization without needing an external magnetic field [2]. Then, a quantized version of the

AHE, the quantum anomalous Hall effect (QAHE), representing the realization of the QHE in the zero magnetic field has come to the forefront [2, 3]. When QAHE is realized, one can observe a plateau of Hall conductance (ρ_{xy}) of e^2/h and a vanishing longitudinal conductance (ρ_{xx}) even at zero magnetic field (Fig. 1)[4]. Then, the realization of the QAHE may lead to the development of low-power-consumption electronics. There are two prerequisites for the observation of the QAHE: the formation of an exchange gap induced by the coupling with the magnetization in or next to the topological insulator (TI) and the precise tuning of E_F into the gap[5]. In detail, to realize QAHE requires four conditions: (1) the system must be 2D; (2) insulating bulk; (3) ferromagnetic ordering; and (4) a non-zero Chern number[6]. Then topological materials holding magnetism can satisfy the conditions [7–9]. Until now, QAHE state has only been realized in magnetically doped Cr- and/or V-doped $(\text{Bi,Sb})_2\text{Te}_3$ topological insulator films system, below $\sim 1\text{K}$ [4, 10]. However, such a low critical temperature severely constrains both the exploration of fundamental physics and technological applications based on this exotic phenomenon[11]. Therefore, seeking new materials to realize QAHE at higher temperature has

*Corresponding author

**Corresponding author

✉ jingqiang@sdut.edu.cn (Q. Jing); liub@sdut.edu.cn (B. Liu)

ORCID(s):

become a major research direction in the field of topological quantum materials. One approach is to try to dop the other 3d elements such Mn, Fe and Co into the TI. The opening of the gap has been realized in Fe or Mn-doped Bi_2Se_3 [12, 13]. For Co doped TI, ferromagnetic behaviour and antiferromagnetic behaviour have been observed in $\text{Bi}_{1-x}\text{Co}_x\text{Se}_3$ [14, 15] and $\text{Sb}_{2-x}\text{Co}_x\text{Te}_3$ [16], respectively. Another approach is to use the magnetic proximity effects (MPEs) to induce magnetic order in a TI by coupling it to an adjacent magnetically ordered material. Lots of excellent works have been done such as the reports on EuS/TI [17–19], $\text{Y}_3\text{Fe}_5\text{O}_{12}/\text{TI}$ [20–22], CrSb/TI [23], $\text{Tm}_3\text{Fe}_5\text{O}_{12}/\text{TI}$ [24] and CrSe/TI [25]. Another promising approach is to realize high-temperature QAHE insulator in thin films of intrinsic ferromagnetic (FM) or antiferromagnetic (AFM) TI materials [26]. Nevertheless, despite much theoretical and experimental efforts devoted, there is little progress until the recent discovery of an intrinsic AFM TI MnBi_2Te_4 [27–32]. The growth of MnBi_2Te_4 was first reported by Lee et al. and it was treated as a kind of thermoelectric material at that time [33]. Then, lots of theoretical and experimental work were done to treat MnBi_2Te_4 as a kind of antiferromagnetic topological insulator [27–32]. On experiment, MnBi_2Te_4 could be synthesized through several approaches, but it is not so easy to get the high purity crystalline samples with perfect antiferromagnetic order [32, 34]. Then to understand its growth mechanism become an urgent necessity. In another aspect, it is proposed that MnBi_2Te_4 is just one member of MB_2T_4 -family materials (MB_2T_4 : M = transition-metal or rare-earth element, B = Bi or Sb, T = Te, Se, or S) [28, 35, 36], which have rich topological quantum states. Among them, MnBi_2Te_4 has been grown successfully and tested, but the other materials of this family with dynamically stable structure have not been realized completely until now. Then, understanding the growth mechanism can help researcher to get the single crystals of the other family members too. Recently, Li et al. has reported the growth of high quality MnBi_2Te_4 with perfect antiferromagnetic order [32]. Based on the result of high-resolution high-angle annular dark field scanning transmission electron microscopy (HAADF-STEM), they proposed the growth mechanism of MnBi_2Te_4 was the intercalation of MnTe into Bi_2Te_3 [37]. Be synchronous with their work, we have grown high quality MnBi_2Te_4 single crystal with perfect antiferromagnetic order too. Our experiences in the synthesis of layered iron-based superconductor ThFeAsN , ThCoAsN , ThMnAsN et.al. [38–40] with ThN layer as the block layer inspire us to consider that the growth mode of MnBi_2Te_4 may be the layer-inserting growth mode. To check it, the chemical states of MnBi_2Te_4 and $\alpha\text{-MnTe}$ were investigated by XPS combing with the Ar^+ ion sputtering. However, the measurement result supports our guess. Understanding the growth mode of MnBi_2Te_4 can help us to grow the other members of MB_2T_4 -family materials. Recently, there are new research progress on the intrinsic magnetic topological insulator and QAHE too. There are several reports on the van-der-Waals-gap inserting growth of $(\text{MnBi}_2\text{Te}_4)(\text{Bi}_2\text{Te}_3)_m$ i.e. inserting Bi_2Te_3 to the van der

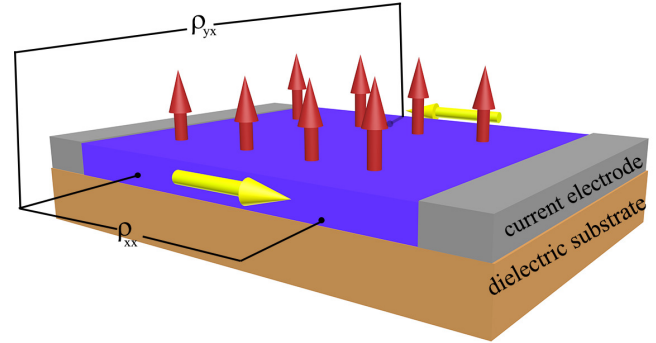


Figure 1: A schematic diagram depicting the principle of QAHE based on a topological insulator thin film owing ferromagnetism. The red arrows have directed the magnetization direction (M). The yellow arrows denote the currents, which are from the conducting edge channel of the device.

Waals gap of MnBi_2Te_4 [41–44]. With the increasing of m , the interlayer antiferromagnetic exchange coupling of $(\text{MnBi}_2\text{Te}_4)(\text{Bi}_2\text{Te}_3)_m$ becomes gradually weakened, as the separation of magnetic layers increases. With $m=3$, it shows long-range ferromagnetic order below 10.5 K, with the easy axis along the c axis [44]. At the same time, the zero-field QAHE has been realized in pure MnBi_2Te_4 at 1.4K by Deng et. al., recently [45].

2. Experimental Section

2.1. Growth of MnBi_2Te_4 Single Crystals

Bi powder (99.99%), Te powder (99.999%) and Mn powder (99.9%) were all bought from Aladdin Company of China. $\alpha\text{-MnTe}$ polycrystalline samples were prepared by mixing the powder components of Mn and Te in an atomic ratio 1:0.97. Then the mixture was placed in an Al_2O_3 crucible and sealed in an evacuated quartz tube. The quartz tube was initially heated up to 700°C at a rate of $2^\circ\text{C}/\text{h}$, holding at this temperature for one day followed by water quenching. The growth process of Bi_2Te_3 is as following: Bi powder and Te powder were mixed according to the stoichiometric ratio. Then the mixture was placed in an Al_2O_3 crucible and sealed in an evacuated quartz tube. The quartz tube was initially heated up to 850°C in 5 hours and then kept at this temperature for about 20 hours. Next, the temperature was decreased to 550°C in 48 hours. After that it was kept at 550°C for 5 days then the heating program was closed. After that the Bi_2Te_3 single crystal was gotten and then was smashed into powder to be utilized as precursor. High quality single crystals of MnBi_2Te_4 were synthesized using the flux method. The raw materials of $\alpha\text{-MnTe}$ and Bi_2Te_3 were mixed in the molar ratio of 1: 5.85 in an Al_2O_3 crucible, which were sealed inside a quartz ampule. The ampule was put into a furnace and heated to 950°C over a period of one day. After maintaining it at 950°C for 12h, the ampule was cooled to 580°C at a rate of $10^\circ\text{C}/\text{h}$. Large-sized MnBi_2Te_4 crystals were obtained after centrifuge in order to remove the

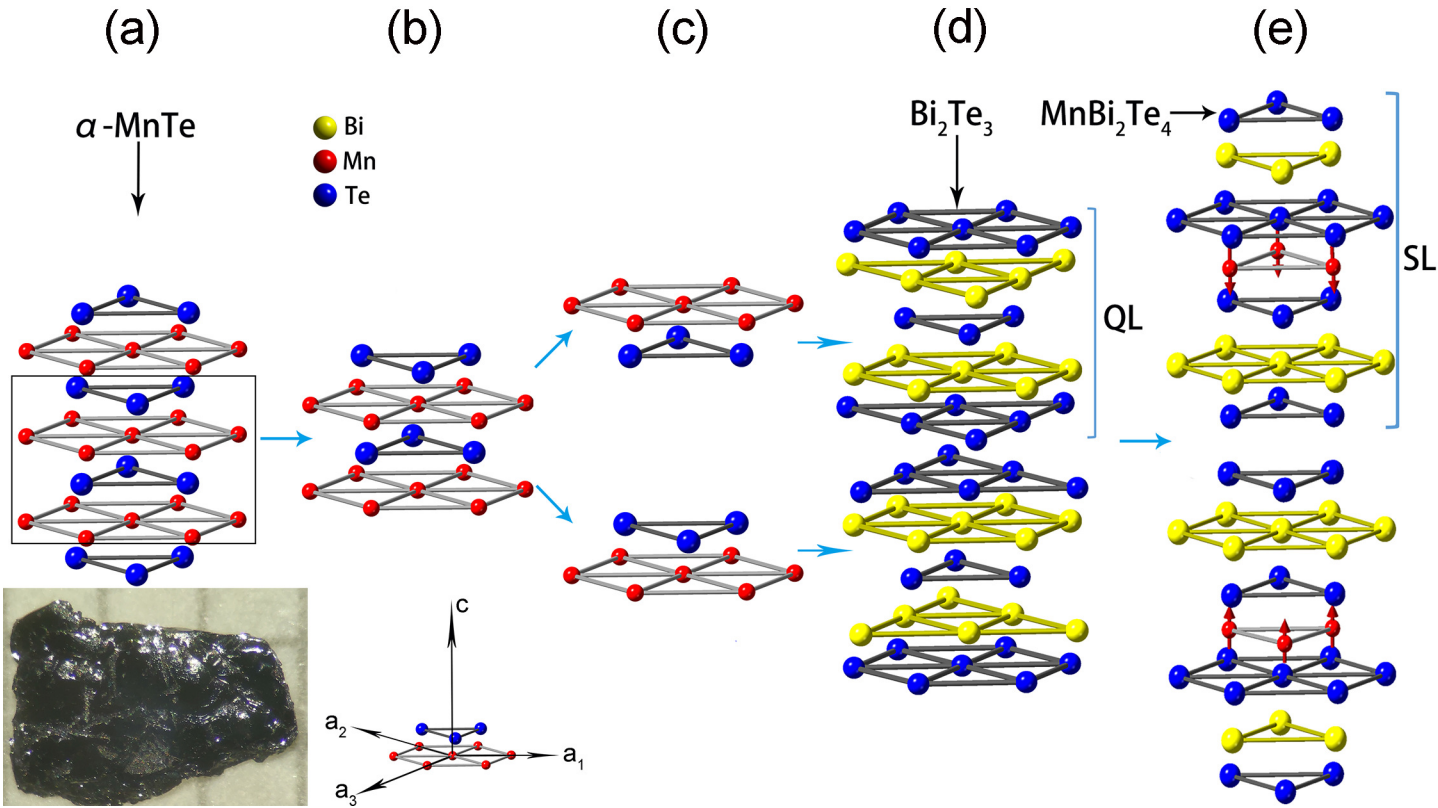


Figure 2: The illustration of layer-inserting growth process of MnBi_2Te_4 . MnBi_2Te_4 includes seven atoms in a unit cell, forming a Te-Bi-Te-Mn-Te-Bi-Te septuple layer (SL). The inserted part of the figure is the single crystal of MnBi_2Te_4 . It is about $3 \times 1.5 \text{mm}^2$ in dimension.

excess Bi_2Te_3 flux.

2.2. Physical Properties Measurements

XPS were performed on Axis Ultra of Kratos Analytical with $\text{AlK}\alpha$ ($h\nu=1486.6 \text{ eV}$) as the monochromatic X-ray radiation source. The electron analyzer pass energy was fixed at 30 eV . The pressure in the spectrometer chamber was maintained at about $8 \times 10^{-10} \text{ Pa}$. The binding energy (BE) scale was referenced to the energy of the C1s peak of adventitious carbon, $E_B=284.8 \text{ eV}$. All peaks had been fitted using a Shirley background and Voigt (mixed Lorentzian-Gaussian) line shapes. In order to remove the surface contamination and oxidation layer, then to observe the intrinsic chemical states of $\alpha\text{-MnTe}$ and MnBi_2Te_4 , sputtering procedure was done by utilizing the Argon ion gun. For both bulk single crystal MnBi_2Te_4 and polycrystal $\alpha\text{-MnTe}$, about 200 nm -thick-film were removed within 180 s . For the Argon ion gun, the estimated sputtering rate is about 1.1 nm/sec and the ion energy is 1000 eV . The analysis software CasaXPS is used to fit the peaks. The magnetization measurements were performed in a Quantum Design superconducting quantum interference device vibrating sample magnetometer system (SQUID-VSM).

3. Results and Discussion

3.1. Crystal Structure and XRD Result

Bi_2Te_3 with rhombohedral crystal structure (trigonal phase) belongs to the space group of D_{3d}^5 ($R\bar{3}m$), with five-atom layers arranging along the c -direction in one unit cell forming a Te-Bi-Te-Bi-Te quintuple layer. The coupling is strong between two atomic layers within one quintuple layer but much weaker, predominantly of the van der Waals type, between two quintuple layers [46]. Sharing the isostructure with Bi_2Te_3 , MnBi_2Te_4 crystallizes in a rhombohedral layered structure belonging to $R\bar{3}m$ space group too. Similar with Bi_2Te_3 , each layer of a unit cell has a triangular lattice with atoms ABC stacked along the c axis [26, 34]. Slightly differently, monolayer MnBi_2Te_4 includes seven atoms in a unit cell, forming a Te-Bi-Te-Mn-Te-Bi-Te septuple layer (SL), which can be viewed as intercalating a Mn-Te bilayer into the center of a Bi_2Te_3 quintuple layer (QL) (Fig.2). As shown in the experimental section, the MnBi_2Te_4 is synthesized by self-flux method, through mixing $\alpha\text{-MnTe}$ and Bi_2Te_3 together, using Bi_2Te_3 as the flux agent. After being heated to 950°C and held for one day, the mixture are cooled slowly to 580°C . During the crystal growth process, the MnTe layers inserts into the Bi_2Te_3 layers and then MnBi_2Te_4 single crystal are gotten. Here, we can use some theories summarized for layered iron-based superconductors to help

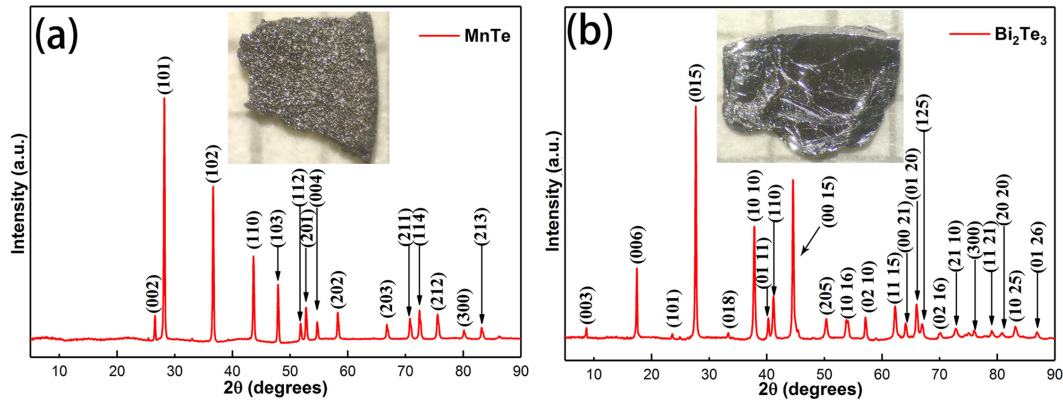


Figure 3: (a) and (b) are the powder XRD pattern of α -MnTe and Bi_2Te_3 , respectively. The inserted part of (a) and (b) are the crystal morphology of α -phase MnTe polycrystals and Bi_2Te_3 single crystal, respectively.

us to understand the layer-inserting growth of MnBi_2Te_4 [47]. It may follow such key points: I) The inserting layers (MnTe bilayer) and the inserted layers (Bi_2Te_3) share the similar crystal structure. Bi_2Te_3 with trigonal phase belongs to $R\bar{3}m(166)$ space group, while α -MnTe with hexagonal phase belongs to $P6_3/mmc(194)$ space group, which is stable in bulk form. As shown by Fig.2 that, both unit cells of α -MnTe and Bi_2Te_3 have layered structure, with the trigonal layer and hexagonal layer alternately stacking along the c axis, which makes the insertion of -Mn-Te- possible. However, it is predicted that rhombohedral MnBi_2Se_4 ($R\bar{3}m(166)$ space group) is also a kind of antiferromagnetic topological insulator[35]. We have tried several times to get the bulk rhombohedral structure MnBi_2Se_4 by the similar inserting method, but it is not successful. What we have done is that, we use α -MnSe of NaCl structure ($Fm\bar{3}m$ space group of cubic system and the stable phase of manganese selenium compounds) as the inserting layer material to try to insert it into the rhombohedral Bi_2Se_3 . Then it can be explained from the symmetry perspective: inserting α -MnSe with NaCl structure into rhombohedral (trigonal phase) Bi_2Se_3 , just like inserting a square into a stack of triangle (or regular hexagon), which is not permitted by the symmetry and not stable too. We think the symmetry is the major obstacle to hinder the formation of rhombohedral MnBi_2Se_4 which is a potential antiferromagnetic topological insulator. II) Lattice mismatch between α -MnTe and Bi_2Te_3 is acceptable. According to the powder XRD pattern shown by Fig.3, we have refined lattice parameters of α -MnTe which are $a=4.1477 \text{ \AA}$, $c=6.7123 \text{ \AA}$, while for that of Bi_2Te_3 are $a=4.384 \text{ \AA}$, $c=30.488 \text{ \AA}$, respectively. As the lattice parameters mainly influencing the inserting process is from a axis, the lattice mismatch between α -MnTe and Bi_2Te_3 in a axis is calculated, which is only 3.4% ($\frac{a-a_0}{a} \times 100\%$). III) Self-stability of α -MnTe. The bulk α -phase of MnTe is stable at room temperature and atmospheric pressure. IV) There exists charges transfer between the inserting layers (MnTe) and the inserted layers (Bi_2Te_3). As shown by Fig.2 (c), (d) and (e) that, during the inserting growth process bilayer -Mn-Te- of α -MnTe would insert into the gap between the third layer (Te atoms layer) and fourth

layer (Bi atoms layer) of the unit quintuple layer of Bi_2Te_3 . Therefore, Mn atoms of α -MnTe would bond with Te atoms of Bi_2Te_3 , then Mn atoms would transfer electrons to Te; Te atoms of α -MnTe would bond with Bi atoms of Bi_2Te_3 , then Bi atoms would transfer electrons to Te. The charges transfer can make the MnBi_2Te_4 system stable. In summary, the growth mode of MnBi_2Te_4 has typical character of inserting layer mode.

3.2. Magnetic and Transport Properties

Fig.4 (a) shows the temperature dependent magnetic susceptibility of MnBi_2Te_4 single crystal measured at 10000Oe. It could be observed that MnBi_2Te_4 shows antiferromagnetic behaviour with $T_N = 24.5\text{K}$. Meanwhile, a strongly anisotropic magnetic susceptibility is observed. The magnetic susceptibility of H//c displays much steeper transition below 24.5K, which means the c axis is the easy axis. A modified Curie-Weiss law $\chi(T) = \chi_0 + C/(T - \Theta_{cw})$ is used to fit the paramagnetic regime above T_N in the range of 30 K to 300 K. Here, χ_0 means a temperature-independent magnetic susceptibility, which contains two parts: one is diamagnetism closed electron shells; the other one is the Pauli paramagnetism due to the metallicity of MnBi_2Te_4 . The temperature-dependent Curie-Weiss susceptibility $C/(T - \Theta_{cw})$ is mainly from localized Mn moments. The fitted effective paramagnetic moment with the value of $5.0\mu_B$ roughly agrees with the high-spin configuration of Mn^{2+} ($S = 5/2$)[29]. Meanwhile, the Curie-Weiss temperature $\Theta_{cw} = 3.1\text{K}$ strongly depends on the fitted χ_0 contribution. Below T_N , a spin-flop transition at $H \approx 35000 \text{ Oe}$ is observed for H//c (Fig. 4b) in the M-H curve, which is in line with the M-T result suggesting that c axis is the easy axis. To check its magnetic properties further, field dependence of magnetization of MnBi_2Te_4 single crystal has been measured at different temperatures under the magnetic field of H//c and H \perp c. Its temperature dependence of magnetic susceptibility has been measured under magnetic field too(see Fig.S1 of the Supplementary materials). As shown by Fig.S1 (a) that, for H//c, above T_N , the magnetization displays a linear dependence, indicating the paramagnetic state; below T_N , all the curves show spin-flop

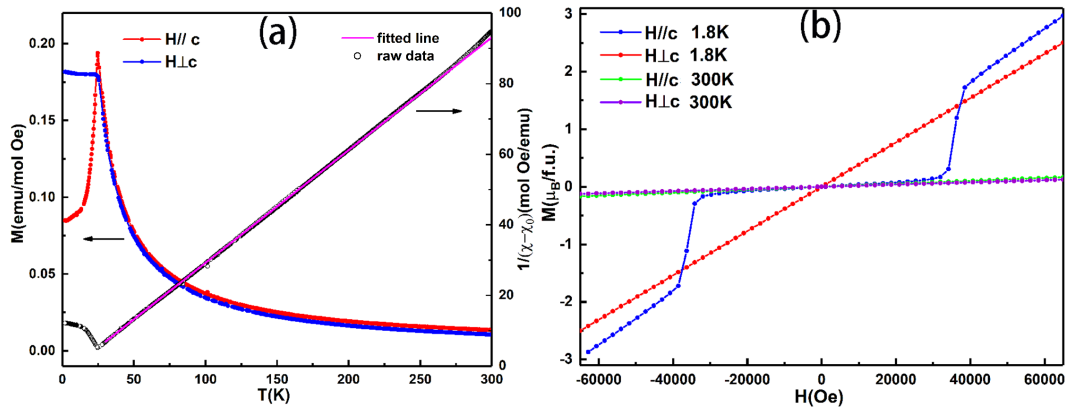


Figure 4: (a) The left axis of ordinates shows the magnetic susceptibility of MnBi_2Te_4 as a function of temperature measured in an external magnetic field of $H=10000\text{Oe}$ in zero-field-cooled (zfc) mode. The right axis of ordinates shows the temperature dependent reciprocal susceptibility of $H//c$. The pink line is a fitted line according to modified Curie-Weiss law, fitted in the range of 30 K to 300 K ($\chi_0=0.0029$ emu/mol Oe). (b) Field-dependent magnetization curves for two directions measured at 1.8K and 300 K.

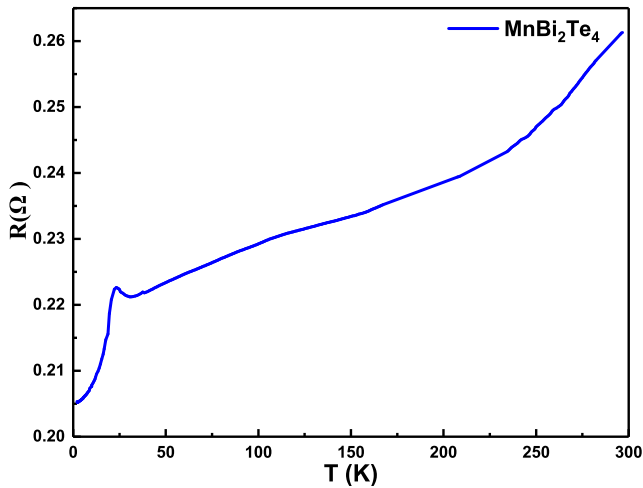


Figure 5: Temperature dependence of resistance of MnBi_2Te_4 single crystal measured from 2K to room temperature.

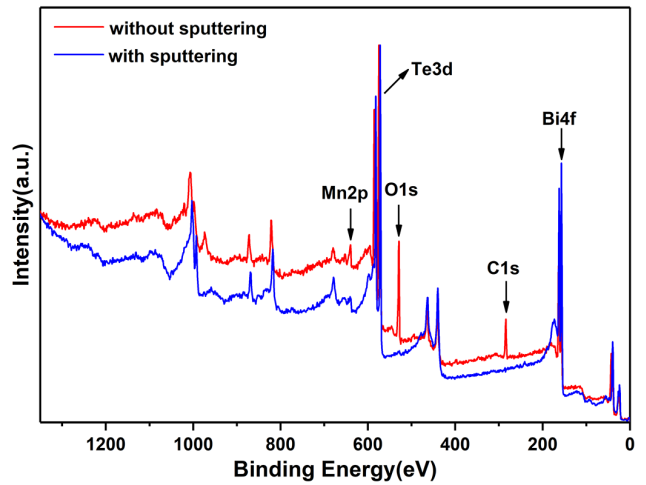


Figure 6: Survey XPS spectra acquired from the MnBi_2Te_4 surface. After sputtering, there exists no contaminants, i.e. oxygen and carbon anymore.

transition. As shown by Fig.S1 (c) that, the antiferromagnetic transition tends to become weaker and finally disappears with the increase of the applied out-of-plane magnetic field, due to the suppression and spin-flop of interlayer antiferromagnetic coupling caused by the external out-of-plane magnetic field[30, 32]. The magnetic measurement result shows that the MnBi_2Te_4 single crystal owns good crystal quality and well antiferromagnetic property. As shown by Fig.5, complementary to the magnetic measurements, the temperature dependence of the in-plane electrical resistance $R(T)$ of a bulk MnBi_2Te_4 single crystal was measured from room temperature down to $T = 2.0$ K. The resistance decreases with lowering the temperature, which is the metallic behaviour. The R - T curve exhibits a distinct peaklike feature centered at 24.0 K. The local increase indicates an enhanced electron scattering in the vicinity of a magnetic phase transition, and a sharp decrease below the peak signals the

freezing-out of the scattering due to an onset of long-range magnetic order, respectively [31, 48]. This is consistent with the magnetic measurement result.

3.3. XPS Result

The sputtering procedure is done to remove the surface contaminants of MnBi_2Te_4 (001). As illustrated by Fig. 6, compared to the initial spectrum (above line), the spectrum obtained from the cleaned surface (below line) does not show surface contaminants, i.e. oxygen and carbon anymore. Fig. 7 shows the XPS spectrum of Mn2p and Te3d. Their fitted parameters are shown in Table I. Deconvolution of the Mn2p spectrum of Fig. 7(a) reveals two main contributions: Peak 1 at the position of 640.8eV and Peak 2 with $E_B=642.1$ eV. Compared with the reference data [49], it is found that Peak 2 corresponds to Mn-O bond of MnO_2 . Considering

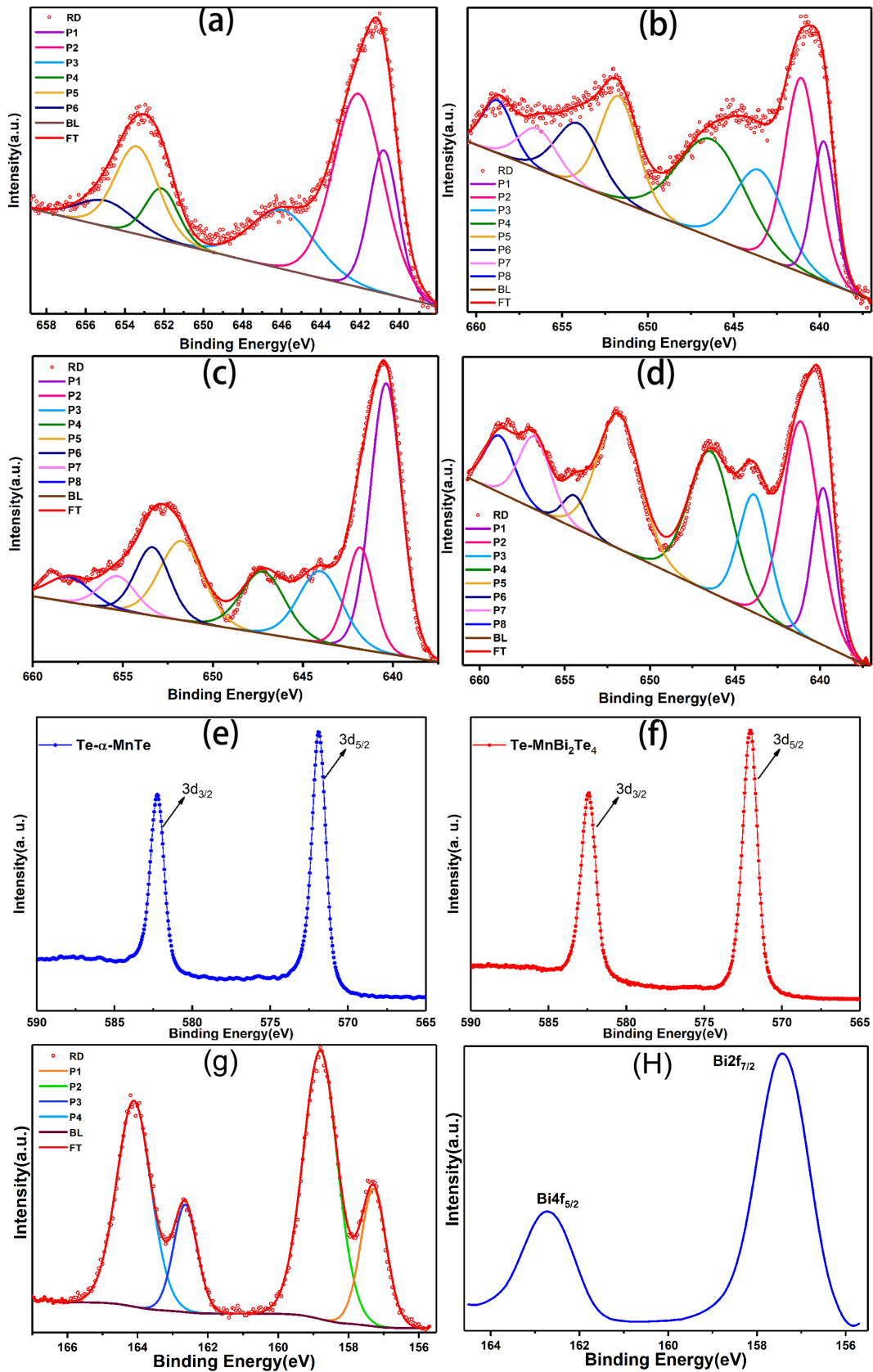


Figure 7: (a) and (b) are the XPS spectra of Mn2p core-level acquired from α -MnTe, without and with sputtering, respectively. (c) and (d) are the XPS spectra of Mn2p core-level acquired from the MnBi₂Te₄ surface without and with sputtering, respectively. (e) and (f) are the XPS spectra of Te3d obtained from sputtered α -MnTe and MnBi₂Te₄, respectively. (g) and (h) are the XPS spectra of Bi4f core-level acquired from the MnBi₂Te₄ surface without and with sputtering, respectively. For all the panels, the peaks are numbered increasingly from right to left as Peak1 (P1), Peak 2 (P2), Peak 3 (P3), Meanwhile, RD denotes the raw data; BL means the base line; FT corresponds to the fitted line.

Table I

shows the fitted peaks' position of Mn2p and Te3d of α -MnTe and MnBi₂Te₄, respectively. 'S' denotes sputtering; 'WTS' means without sputtering

Mn2P _{3/2}	MnTe	WTS	P1	640.8	MnO and MnTe
		S	P1	639.8	Mn subtelluride
		WTS	P2	642.1	MnO ₂
		S	P2	641.1	MnTe
		WTS	P3	646.1	Satellite of P1
		S	P3	643.5	Satellite of P1
	MnBi ₂ Te ₄	WTS	P4	646.3	Satellite of P2
		WTS	P1	640.6	MnO and MnTe
		S	P1	639.8	Mn subtelluride
		WTS	P2	642.1	MnO ₂
		S	P2	641.1	MnTe
		WTS	P3	644.2	Satellite of P1
		S	P3	643.9	Satellite of P1
		WTS	P4	647.4	Satellite of P2
Te3d _{5/2}	MnTe	S	571.9	Mn-Te	
	MnBi ₂ Te ₄	S	572.0	Mn-Te	
Bi4f _{7/2}	MnBi ₂ Te ₄	WTS	P1	157.3	Bi-Te
		WTS	P2	158.8	Bi ₂ O ₃
		S		157.4	Bi-Te

the overlap of the binding energy of MnO and MnTe[50], Peak 1 of Fig.7 (a) may be a sum of two partial contributions: MnO and MnTe. However, it is difficult to separate Peak 1 into two reasonable parts. Peak 3 shifting to higher energies can be ascribed to the satellite of Peak 1[50–54]. The satellites are also called shakeup satellites. It locates at the higher-binding-energy side of the relevant core-lines of transition metal (TM) or rare earth (RE) ions in the selected TM or RE compounds [55]. It also concerns on particular binary Mn oxides, especially MnO [54]. Such satellite structure in Mn 2p XPS spectrum originates from charge transfer between outer electron shell of ligand and an unfilled 3d shell of Mn during creation of core-hole in the photoelectron process [52–54]. For Fig.7 (c), Peak 1 at the position of 639.8eV corresponds to +1 charge state of Mn, which may come from nanoclusters of manganese subtelluride (possibly Mn₂Te) induced by Ar⁺ ion sputtering[50]. The above effect is strictly analogous to the reduction of Mn oxides during Ar⁺ ion bombardment[56]. Peak 3 with the binding energy of 643.5 eV is supposed to be the satellite of Peak 1. Peak 2 at the position of 642.1eV belongs to Mn-O bonds of MnO₂. Peak 4 is the satellite of Peak 2. For (b) and (d) panels of Fig.6, the removal of contaminants from the surface leads to disappearance of the native oxides contributions to the Mn2p spectrum, i.e. those of MnO₂ and MnO. Therefore, Peak 2 of Fig. 7(d), with $E_B=641.1$ eV, can be ascribed to the divalent Mn-Te bond of MnBi₂Te₄. Peak 4 of Fig. 7(d) exhibiting a shift from Peak 2 with the value of $\Delta E=E_{p4}-E_{p2}=5.3$ eV (as shown by Table I) is the satellite of Peak 2. Peak 1 with E_B

= 639.8 eV may be induced by the Ar⁺ ion bombardment during the surface preparation. It is the +1 charge state of Mn and can be ascribed to the Mn–Te bond in the nanoclusters of manganese subtelluride (possibly Mn₂Te), created in the surface and subsurface region penetrated by Ar⁺ ions [33]. Peaks 3 is the corresponding satellite of Peak 1. In addition, rising intensity of the Mn2p satellite for divalent Mn (bound to chalcogen) with atomic number of ligand (from MnO to MnBi₂Te₄) could be observed too. As shown by Fig. 7 (e) and (f) that the peaks' positions of Te3d of α -MnTe almost overlap with those of MnBi₂Te₄, which means that the chemical states of Te both from α -MnTe and MnBi₂Te₄ are the same. Fig. 7 (g) and (h) are the XPS spectra of Bi4f acquired from the MnBi₂Te₄ surface without and with sputtering, respectively. As shown by Fig.7(g) that peak 1 locating at the position of 157.3eV corresponds to Bi-Te bond, while peak 2 locating at the position of 158.8eV corresponds to Bi-O bond of Bi₂O₃[57, 58]. As shown by Fig.7(h) that, after being sputtered, there exists only one kind of bond i. e. Bi-Te bond with the binding energy of 157.4eV. This tells us again that the contaminants have been removed completely by the sputtering procedure. Comparison of the fitted Mn2p and Te3d parameters of the MnBi₂Te₄ and α -MnTe spectral components gathered in Table I, it shows a very good consistency between them (considering the accuracy of the method, i.e. $\Delta E = 0.1$ eV). Then we can get the conclusion that, Mn and Te of MnBi₂Te₄ share the same chemical state with those of α -MnTe, which supports our hypothesis that the growth mode of MnBi₂Te₄ is the inserting-layer growth mode.

4. Conclusion

Single crystals of antiferromagnetic topological insulator MnBi₂Te₄ have been grown by flux method. The magnetic property of MnBi₂Te₄ is investigated, which shows good antiferromagnetic character with Neel temperature of 24.5K and a spin-flop transition at $H \approx 35000$ Oe, 1.8K. The possible inserting-layer growth mode of MnBi₂Te₄ is proposed, which is supported by the XPS and XRD result of α -MnTe and MnBi₂Te₄. The proposed crystal growth mechanism may help us to grow the other members of MB₂T₄-family materials, which have rich topological quantum states.

The XPS measurement combing with the Ar⁺ ion sputtering is done to investigate chemical states of MnBi₂Te₄ and α -MnTe. Binding energies of MnBi₂Te₄-related contributions to the Mn2p and Te3d spectra agree well with those of α -MnTe.

5. Acknowledgements

This work was supported by the Natural Science Foundation of Shandong Province, China (Nos. ZR2016AQ08, ZR2019MA036) and National Natural Science Foundation of China (Nos. 11804194).

References

- [1] K. He, Y.Y. Wang, and Q.K. Xue. Quantum anomalous hall effect. *Nat. Sci. Rev.*, 1(1):38–48, 2014.
- [2] N. Nagaosa, J. Sinova, and S. Onoda. Anomalous hall effect. *Rev. Mod. Phys.*, 82(2):1539, 2010.
- [3] M. Onoda and N. Nagaosa. Quantized anomalous hall effect in two-dimensional ferromagnets: quantum hall effect in metals. *Phys. Rev. Lett.*, 90(20):206601, 2003.
- [4] C.Z. Chang et al. Experimental observation of the quantum anomalous hall effect in a magnetic topological insulator. *Science*, 340(6129):167–170, 2013.
- [5] Y. Tokura, K. Yasuda, and A. Tsukazaki. Magnetic topological insulators. *Nat. Rev. Phys.*, 1(2):126–143, 2019.
- [6] H.M. Weng, X. Dai, and Z. Fang. From anomalous hall effect to the quantum anomalous hall effect. *AAPPS Bulletin*, 3(23), 2013.
- [7] R. Yu, W. Zhang, and H.J. Zhang et al. Quantized anomalous hall effect in magnetic topological insulators. *Science*, 329(5987):61–64, 2010.
- [8] C.Z. Chang and M. Li. Quantum anomalous hall effect in time-reversal-symmetry breaking topological insulators. *J. Phys. Condens. Matter.*, 28(12):123002, 2016.
- [9] K. He, Y. Wang, and Q.K. Xue. Topological materials: quantum anomalous hall system. *Annu. Rev. Condens. Matter. Phys.*, 9:329–344, 2018.
- [10] C.Z. Chang et al. High-precision realization of robust quantum anomalous hall state in a hard ferromagnetic topological insulator. *Nat. Mater.*, 14(5):473–477, 2015.
- [11] S.H. Lee, Y.L. Zhu, Y. Wang, and L.X. Miao. Spin scattering and noncollinear spin structure-induced intrinsic anomalous hall effect in antiferromagnetic topological insulator MnBi_2Te_4 . *Phys. Rev. Res.*, 1(1):012011, 2019.
- [12] S.Y. Xu, N. Madhab, C. Liu, D.M. Zhang, R. Anthony, and W. L. Andrew et al. Hedgehog spin texture and berry's phase tuning in a magnetic topological insulator. *Nat. Phys.*, 8(8):616–622, 2012.
- [13] Y.L. Chen, J.H. Chu, J.G. Analytis, and Z.K. Liu et al. Massive dirac fermion on the surface of a magnetically doped topological insulator. *Science*, 329(5992):659–662, 2010.
- [14] I. Bushra and C. Ratnamala. Magneto-transport and Kondo effect in cobalt doped Bi_2Se_3 topological insulators. *Appl. Phys. Lett.*, 107(17):173108, 2015.
- [15] S. Rahul, K.K. Shukla, A. Kumar, and G.S. Okram et al. Large power factor and anomalous Hall effect and their correlation with observed linear magneto resistance in Co-doped Bi_2Se_3 3D topological insulator. *J. Phys. Condens. Matter*, 28(37):376001, 2016.
- [16] S. Abhishek, A.K. Ghosh, and C. Sandip. Antiferromagnetic Ordering at Room Temperature in Co-Doped Sb_2Te_3 Topological Insulators. *J. Supercond. Nov. Magn.*, 31(2):299–305, 2018.
- [17] W. Peng, K. Ferhat, A. Badih, and S. Hadar et al. Exchange-coupling-induced symmetry breaking in topological insulators. *Phys. Rev. Lett.*, 110(18):186807, 2013.
- [18] C. Lee, K. Ferhat, and J. H. Pablo et al. Direct measurement of proximity-induced magnetism at the interface between a topological insulator and a ferromagnet. *Nat. Commun.*, 7(1):1–6, 2016.
- [19] K. Ferhat, L. Valeria, N. Flavio, A. Badih, and J. Michelle et al. A high-temperature ferromagnetic topological insulating phase by proximity coupling. *Nature*, 533(7604):513–516, 2016.
- [20] L. Murong, M. Mohammad, O. Mehmet, X.F. Kou, and Y.B. Fan et al. Proximity induced high-temperature magnetic order in topological insulator-ferromagnetic insulator heterostructure. *Nano. Lett.*, 14(6):3459–3465, 2014.
- [21] Z.L. Jiang, C. Z. Chang, C. Tang, and J.G. Zheng et al. Structural and proximity-induced ferromagnetic properties of topological insulator-magnetic insulator heterostructures. *AIP Adv.*, 6(5):055809, 2016.
- [22] X.Y. Che, M. Koichi, P. Lei, H.Q. Lin, and G.Q. Yu et al. Proximity-induced magnetic order in a transferred topological insulator thin film on a magnetic insulator. *ACS Nano.*, 12(5):5042–5050, 2018.
- [23] Q.H. Lin, X.F. Kou, G. Alexander, Y. Gen, and P. Lei et al. Tailoring exchange couplings in magnetic topological-insulator/antiferromagnet heterostructures. *Nat. Mater.*, 16(1):94–100, 2017.
- [24] C. Tang, C. Z. Chang, G.J. Zhao, Y. W. Liu, and Z.L. Jiang et al. Above 400-k robust perpendicular ferromagnetic phase in a topological insulator. *Sci. Adv.*, 3(6):e1700307, 2017.
- [25] C.Y. Yang, L. Pan, G. Alexander, H.Y. Wang, and X.Y. Che et al. Termination switching of antiferromagnetic proximity effect in topological insulator. *Sci. Adv.*, 6(33):eaaz8463, 2020.
- [26] P. Tang, Q. Zhou, G. Xu, and S.C. Zhang. Dirac fermions in an antiferromagnetic semimetal. *Nat. Phys.*, 12(12):1100–1104, 2016.
- [27] D. Zhang, M. Shi, T. Zhu, D. Xing, H. Zhang, and J. Wang. Topological axion states in magnetic insulator MnBi_2Te_4 with the quantized magnetoelectric effect. *Phys. Rev. Lett.*, 122(20):206401, 2019.
- [28] J. Li, Y. Li, S. Du, and Z. Wang et al. Intrinsic magnetic topological insulators in van der waals layered MnBi_2Te_4 -family materials. *Sci. Adv.*, 5(6):eaaw5685, 2019.
- [29] M.M. Otrokov, Mikhail M, and Klimovskikh et al. Prediction and observation of an antiferromagnetic topological insulator. *Nature*, 576(7787):416–422, 2019.
- [30] J.Q. Yan et al. Crystal growth and magnetic structure of MnBi_2Te_4 . *Phys. Rev. Mater.*, 3(6):064202, 2019.
- [31] A. Zeugner et al. Chemical aspects of the candidate antiferromagnetic topological insulator MnBi_2Te_4 . *Chem. Mater.*, 31(8):2795–2806, 2019.
- [32] H. Li et al. Antiferromagnetic topological insulator MnBi_2Te_4 : Synthesis and magnetic properties. *Phys. Chem. Chem. Phys.*, 22(2):556–563, 2020.
- [33] A. Aoki et al. X-Ray Photoelectron Spectroscopic Studies on ZnS : MnF_2 Phosphors. *Jpn. J. Appl. Phys.*, 15(2):305, 1976.
- [34] D.S. Lee, T.H. Kim, C.H. Park, C.Y. Chung, Y.S. Lim, W.S. Seo, and H.H. Park. Crystal structure, properties and nanostructuring of a new layered chalcogenide semiconductor, Bi_2MnTe_4 . *CrystEngComm.*, 15(27):5532–5538, 2013.
- [35] S. Chowdhury, F. Kevin, Garrity, and F. Tavazza. Prediction of weyl semimetal and antiferromagnetic topological insulator phases in Bi_2MnSe_4 . *NPI. Comput. Mater.*, 5(1):1–7, 2019.
- [36] S.V. Eremeev, M.M. Otrokov, and E.V. Chulkov. Competing rhombohedral and monoclinic crystal structures in MnPn_2Ch_4 compounds: An ab-initio study. *J. Alloy. Compd.*, 709:172–178, 2017.
- [37] H. Li, S.S. Liu, C. Liu, J.S. Zhang, and Y. Xu. Antiferromagnetic topological insulator MnBi_2Te_4 : synthesis and magnetic properties. *Chem. Phys.*, 22(2):556–563, 2020.
- [38] C. Wang, Z.C. Wang, Y.X. Mei, and Y.K. Li et al. A new ZrCuSiAs -type superconductor: ThFeAsN . *J. Am. Chem. Soc.*, 138(7):2170–2173, 2016.
- [39] J.F. Wang, F. Jiao, X.Y. Wang, S. Zhu, L.B. Cai, C.H. Yang, P.W. Song, F.X. Zhang, B.Z. Li, Y.L. Li, J.Y. Hu, S.B. Li, Y.Q. Li, S.G. Tan, Y.X. Mei, Q. Jing, B. Liu, C. Wang, and D. Qian. The phase transition of $\text{ThFe}_{1-x}\text{Co}_x\text{AsN}$ from superconductor to metallic paramagnet. *EPL*, 130(6):67003, 2020.
- [40] F.X. Zhang, B.Z. Li, Q.Y. Ren, and H.C. Mao et al. ThMnPnN ($\text{Pn} = \text{P}, \text{As}$): Synthesis, Structure and Chemical Pressure Effects. *Inorg. Chem.*, 59(5):2937–2944, 2020.
- [41] I.I. Klimovskikh, M.M. Otrokov, D. Estyunin, Se.V. Eremeev, and S.O. Filnov et al. Tunable 3D/2D magnetism in the $(\text{MnBi}_2\text{Te}_4)(\text{Bi}_2\text{Te}_3)_m$ topological insulators family. *npj Quantum Materials*, 5(1):1–9, 2020.
- [42] M. Z. Shi, B. Lei, C. S. Zhu, D. H. Ma, and J. H. Cui et al. Magnetic and transport properties in the magnetic topological insulators $\text{MnBi}_2\text{Te}_4(\text{Bi}_2\text{Te}_3)_n$ ($n = 1, 2$). *Phys. Rev. B.*, 100(15):155144, 2019.
- [43] J.Z. Wu, F.C. Liu, M. Sasase, and K. Ienaga et al. Natural van der waals heterostructural single crystals with both magnetic and topological properties. *Sci. Adv.*, 5(11):eaax9989, 2019.
- [44] C.W. Hu, L. Ding, K. N. Gordon, B. Ghosh, H.J. Tien, and H.X. Li et al. Realization of an intrinsic ferromagnetic topological state in $\text{MnBi}_8\text{Te}_{13}$. *Sci. Adv.*, 6(30):eaaba275, 2020.
- [45] Y.J. Deng, Y.J. Yu, M. Z. Shi, and Z.X. Guo and Z.H. Xu et al. Quantum anomalous Hall effect in intrinsic magnetic topological insulator

- MnBi₂Te₄. *Science*, 367(6480):895–900, 2020.
- [46] H.J. Zhang, C.X. Liu, X.L. Qi, X. Dai, Z. Fang, and S.C. Zhang. Topological insulators in Bi₂Se₃, Bi₂Te₃ and Sb₂Te₃ with a single dirac cone on the surface. *Nat. Phys.*, 5(6):438–442, 2009.
- [47] H. Jiang, Y.L. Sun, Z.A. Xu, and G.H. Cao. Crystal chemistry and structural design of iron-based superconductors. *Chin. Phys. B.*, 22(8):087410, 2013.
- [48] C. Hess, A. Kondrat, and A. Narduzzo et al. The intrinsic electronic phase diagram of iron-oxypnictide superconductors. *EPL*, 87(1):17005, 2009.
- [49] J.F. Moulder, W.F. Stickle, and P.E. Sobol and K.D. Bomben. Handbook of X-ray photoelectron spectroscopy. *Physical electronics*, pages 230–232, 1995.
- [50] R.J. Iwanowski and M.H. Heinonen and E. Janik. X-ray photoelectron spectra of zinc-blende MnTe. *Chem.Phys.Lett.*, 387(1-3):110–115, 2004.
- [51] R.J. Iwanowski, M.H. Heinonen, and E. Janik. Sputter cleaning and annealing of zinc-blende MnTe surface—XPS study. *Appl. Surf. Sci.*, 249(1-4):222–230, 2005.
- [52] S.P. Jeng, R.J. Lad, and V.E. Henrich. Satellite structure in the photoemission spectra of MnO(100). *Phys.Rev.B.*, 43(14):11971, 1991.
- [53] J. van Elp, R.H. Potze, H. Eskes, R. Berger, and G.A. Sawatzky. Electronic structure of MnO. *Phys. Rev. B.*, 44(4):1530, 1991.
- [54] M. Oku, K. Wagatsuma, and T. Konishi. Relation between 2p X-ray photoelectron and K_α X-ray emission spectra of manganese and iron oxides. *J. Electron. Spectrosc.*, 98:277–285, 1999.
- [55] J. Park, S. Ryu, M. Han, and S.J. Oh. Charge-transfer satellites in the 2p core-level photoelectron spectra of heavy-transition-metal dihalides. *Phys. Rev. B.*, 37(18):10867, 1988.
- [56] Y. Umezawa and C.N. Reilly. Effect of argon ion bombardment on metal complexes and oxides studied by x-ray photoelectron spectroscopy. *Anal. Chem.*, 50(9):1290–1295, 1978.
- [57] H. Bando, K. Koizumi, Y. Oikawa, and K. Daikohara et al. The time-dependent process of oxidation of the surface of Bi₂Te₃ studied by x-ray photoelectron spectroscopy. *J. Phys. Condens. Matter*, 12(26):5607, 2000.
- [58] T. El Ashram and P. Carapeto Ana et al. Rapidly Solidified Melt-spun Bi-Sn Ribbons: Surface Composition Issues. *J. Adv. Phys.*, 11(5), 2016.